Mapping the Thermal Behavior of the Martian Middle Atmosphere

Terry Z. Martin

Jet Propulsion Laboratory,
4800 Oak Grove Drive,
MS 169-237,
California Institute of Technology,
Pasadena CA 91109 USA

James R. Murphy

New Mexico State University,
4800 Oak Grove Drive,
MS 169-237,
California Institute of Technology,
Pasadena CA 91109 USA

Jeff Hollingsworth

NASA Ames Research Center,
4800 Oak Grove Drive,
MS 169-237,
California Institute of Technology,
Pasadena CA 91109 USA

For submission to Journal of Geophysical Research – Planets, July 2000

Direct correspondence to:

Terry Z. Martin
Mail stop 169-237
Jet Propulsion Laboratory
4800 Oak Grove Dr.
Pasadena CA 91109
(818) 354-2178
FAX: (818) 393-4619
Terry.Z.Martin@jpl.nasa.gov

The Mars Global Surveyor spacecraft horizon sensor, operating at 15 μm, has been mapping global atmospheric thermal behavior continuously since the start of the mapping phase in May 1999. The atmosphere shows consistent longitude-fixed variations in temperature, likely driven by the topography. Strong modifications of the clear-period wave behavior occurred during the dust storm season in 1999, including development of semidiurnal variation in the north. These changes strongly resemble those documented by the Viking IRTM in 1977. The temperature peak moved to the south pole. A second band of high temperatures developed in the north, with a maximum near 11 hrs local time. This band contains travelling waves that are particularly active during the dust storm period.

Introduction

MGS has been the first successful attempt to monitor the Martian atmosphere with a consistent set of observations over a significant part of a Mars year. Few Martian dust storm seasons have been observed directly by spacecraft experiments. Mariner 9 arrived at Mars in 1971 while a truly global storm covered the planet to such a degree that even the high volcanoes were not initially visible. Viking Orbiters 1 and 2 observed some aspects of the start of two major storms in 1977, but their spatial and temporal coverage left an incomplete picture of how those events developed. In all these events, the thermal effects were found to be profound, due to the absorption of sunlight by airborne dust. Any additional information on how dust storms germinate and spread is of value in modelling this uniquely Martian phenomenon.

The Mars Horizon Sensor Assembly (MHSA) is an engineering device intended to provide information to the nadir-aligned Mars Global Surveyor spacecraft attitude control system about the alignment of the vehicle relative to the limb of the planet in four directions 90° apart. At the mean orbit altitude of ~400 km, the large triangular fields of view (Fig. 1) approximately bisect the limb. The MHSA is a direct descendant of many Earth orbital spacecraft instruments (Barnes Eng. Corp., Stamford, CT) that also take advantage of the strong 15 μm CO_2 band, using metal thermopile detectors and no moving parts. The passband used is broad (14 -16 μm), providing adequate signal in the cold polar regions, which can be at ~130 K. In this band, emission arises high in the atmosphere, and the planet appears relatively bland spatially, compared to surface-sensing wavelengths. The corresponding weighting function (Fig. 2) is peaked near the 0.4 mbar level. For limb viewing, there is negligible contribution to the detected radiance from the surface itself in the wings of the band.

The special geometry of the fields of view permits derivation of two useful quantities: the height of the limb within the B field, of primary engineering value, and the radiance of the atmosphere for the fraction of the B field that is on-planet. We employ here the MHSA radiance equation

$$R = C * [(A-S) + (B-S)]^2 /4(A-S)$$

where A, B, and S are the raw signals from the corresponding fields of view (Fig. 1) and C is a calibration coefficient obtained by comparing observations with simultaneous TES spectra crossing the limb during the inter-aerobraking period, when the spacecraft was also nadir-pointed, and passed through the final orbit altitude briefly near periapses. The TES covers the MHSA passband at higher spectral resolution - about 5 cm^{-1}, and with much higher spatial resolution. We believe the absolute accuracy of the brightness temperature to be <5 K, but the more important factor is the high stability of the calibration, owing to the sensor design and the constant referencing to the space signal S. The radiance is converted to brightness temperature for science purposes. Because we compute the limb-relative position of the field of view from other spacecraft engineering sources, we can track the behavior of the limb height calculation and detect when the viability of the radiance calculation is suspect.

Although the TES instrument covers the entire MHSA band at higher resolution, and can therefore derive vertical temperature profiles, the MHSA retains several advantages that make its data invaluable. First, its four quadrants afford spatial and temporal coverage that are beneficial. Transient events may be seen in MHSA data that would not be sensed by the TES until much later. Second, the coverage of the MHSA in local time is broader, due to the sidelooking quadrants, which, due to the nearly polar orbit, are sampling earlier and later in time than the fore and aft quadrants.

Aerobraking phase

During the two long MGS aerobraking phases - Sept. 1997 to May 1998 (L_s 182 to 300°) and Nov. 1998 to March 1999 (L_s 30 to 92°) - the spacecraft was oriented near periapsis with the science instruments pointed aft along the orbit, in order to minimize possible damage from atmospheric friction. As a result, one or more of the MHSA quadrants were swept across the planet, achieving emission angles (spacecraft-surface-normal) typically around 30°. In these passes, the MHSA acted much like a conventional infrared remote-sensing instrument, with filled fields of view. Its signal was converted to radiance and then to brightness temperature by calibrating against on-disk measurements of the Thermal Emission Spectrometer (TES), which aligned its scan mirror to point in the same direction as the MHSA during periapsis pass #43. Space reference information was obtained from a

quadrant that was off-planet during these passes. The large range of radiances observed while moving south from the northern polar region resulted in a calibration of broad utility (Fig. 3).

The periapsis passes covered the planet with diminishing longitudinal separation due to the lowering period. The polar orbit provided a series of portrayals of bulk atmospheric temperature versus latitude. These were of serendipitous value to the aerobraking team in assessing the likelihood that the atmosphere was warming due to dust events. Warming would create a different density profile at the much higher aerobraking altitudes (~110-130 km), and thus possible danger to the spacecraft. In fact, early plots of MHSA signal showed large oscillations of solar panels that came partly into one quadrant's field of view during periapsis. The second phase of aerobraking was carried out at generally lower dynamic pressures in order to avoid excessive forces on the solar panels.

Although the MHSA viewed Mars at other times than periapsis during the aerobraking orbits, the planet was seen at larger distance and with highly varying emission angle, and the rolling spacecraft attitude did not produce systematic coverage useful with the MHSA's large fields of view. Consequently, we have not pursued analysis during those periods.

The primary scientific value of the MHSA aerobraking data lies in the latitudinal temperature variation, and in the changes induced by the dust storm that occurred in late November, 1997 [Christensen et al, 1998]. The general behavior of the northern latitudes sampled in the first aerobraking seasonal range is better provided by later mapping phase data in the following Mars year (see below). However, we mention here two aspects of particular interest: the derivation of longitudinal wave structure obtained simultaneously with accelerometer measurements [Keating et al, 1998], and the thermal behavior of the Nov. 1997 "Noachis" dust storm.

Over a period from L_s 260 to 278° (periapses 101-139), we measured the latitudinal location of the steepest slope of the northern poleward cooling evident in each periapsis pass. This gradient is associated with a westward wind, termed the polar vortex. For some weeks the spacecraft was at periapsis above this vortex, and experienced strong longitudinal density variation, measured by the accelerometer team to have a dominant wave 2 character. We sought to establish whether the middle to lower atmosphere was also varying longitudinally. In fact, we did find evidence of a wave 2 dominated

variation, with a characteristic amplitude of ~3° latitude for wave 2 and ~1° for wave 1 (Fig. 4). We retain the daytime side data near periapsis separately from the incoming night side data because the higher emission angle at night provides a slightly higher sampling in the atmosphere. The character of the northern midlatitudes during the mapping phase shows evidence of travelling waves at this season, so it is not likely that the phase and amplitude are constant, or predictable. This is distinct from the density variation, which was found to have a steady phase for wave 2.

Measurements of the same behavior occurring in the southern polar vortex region during the second aerobraking period showed a dominant wave 1, with an amplitude of ~4° latitude, and a weaker wave 2 component of ~1°. That behavior is relatively stable in time, and appears to be consistent with thermal field variation produced by Tharsis and Hellas in the NASA GCM representation of this season.

Coverage of the planet near the start of the 1997 November dust storm (L_s 224°) consists of tracks extending from +60° north across the pole and down to about -60° latitude. During these passes, the contribution of surface radiance was not negligible, as evidenced by detection of the major volcanos, which project well up into the weighting function, and by the observation of distinct changes as the field passes over deep Valles Marineris. However, the surface contribution is generally a small fraction of the total, and does not affect conclusions drawn about change during the dust storm. The storm produced 10-12K warming in the middle atmosphere across the latitude range from -50 to +60° over a time period of 97 hrs. The increase was most pronounced at the longitudes near 330° where the storm apparently originated in the southern hemisphere [see opacity maps in Christensen, 1998]. The rapidity of the rise suggests that dust transport alone may not be responsible for the change; an enhanced Hadley (cross-equatorial) circulation caused by increased dust in the south could produce such an effect.

Mapping phase.

Once MGS achieved its final orbit in March 1999, the MHSA began to operate in its designed configuration, pointing four quadrants at the limb simultaneously: forward and aft along the orbital path, and on both sides of the track. The on-limb condition results in a somewhat higher weighting

function (Fig. 2), with a mean level at about 0.4 mbar, and consequently less surface contribution. With a 2-hr period, the MHSA builds spatial coverage rapidly, although the fore and aft quadrants are largely redundant. The local time sampling (Fig. 7) is particularly important, in that up to six times of day are available at a given latitude, in contrast to two for TES. Thus, it is possible to measure diurnal behavior that is diagnostic of the presence of dust. In particular, the semidiurnal mode amplitude can be estimated.

We have concentrated our processing on several products: a set of archivable ASCII files containing the raw data number values, radiances, and derived geometry; color maps of nighttime temperatures; and color renditions of temperature vs. latitude and local time. The latter sets have also been expressed as animations, which readily express seasonal change. We have chosen a grid size of 5° in latitude, longitude, and L_s as our standard. The actual spatial size of the trapezoidal on-planet part of the B field is approximately 78 km along the limb, and 550 km in the direction from the limb to the nadir. We compute geometry for the point of intercept of the center of the B field, and when that is off the limb, we use the nearest tangent point on the limb, since the data can still be of value.

The nighttime maps, only a sampling of which can be presented here (Fig. 6) show a variety of consistent features. For most of the Martian year seen so far, there are tropical thermal highs at 30-60° and near 240° west longitude, and corresponding lows at 90° and 300°. When the thermal maximum moves poleward in southern summer, these continue to be the warmest equatorial longitudes. This wave two pattern is undoubtedly a function of the underlying topography, which equatorially is also dominated by wave two. There is also a host of small consistent wave phenomena that change only slowly during the year; few of these are evident in current model output.

Mars was in a cold and relatively dust free state at L_s 120° when mapping began in 1999. As solar flux increases, and/or dust content builds towards L_s 200° and beyond, the broad equatorial warm band widens. At about L_s 225°, this pattern breaks suddenly into a new one with two warm belts – a strong one in the southern midlatitudes, and a northern one near +45°. This pattern is very similar to that measured by the Viking IR Thermal Mapper for the 1977a dust storm during L_s 225-250°, the weaker of the two storms in that year (Martin, 1981). Later, and also like Viking, the peak temperature moves all the way to the pole, at L_s 260°, and is at its

greatest latitudinal extent during L_s 265-270°. By this time, the northern hemisphere has cooled considerably from its warmest state during L_s 230-240°. Also, the southern equatorial latitudes have cooled. It may be that the Hadley cell is most active, producing the most northern warming, when latitudes –30 to -60° are the warmest.

The diurnal behavior (Fig. 7, also a sampling only) is equally intriguing, though due to the orbit there is little variation in the diurnal coverage pattern during the year. Although all four quadrants necessarily use the same calibration, obtained from measurements in only one, there appears little consistent offset between the temperatures in this presentation, a sign that the observed diurnal changes are real. We note here that the diurnal variation at 15 μm shown in Martin (1981) has been called into question due to a possible filter leak in the IRTM filter (Wilson and Richardson, 1999). Such a leak would produce a more surface-like behavior, with a midday peak. The MHSA data do in fact show very little diurnal variation at all latitudes for the part of the year that is cold and low in dust content, lending weight to the leak hypothesis.

A late afternoon peak near 16-17 hrs develops after L_s 210° in the southern midlatitudes, consistent with Viking findings (the IRTM data are more reliable in the warmer-atmosphere dust storm season). As the behavior changes rapidly at L_s 225°, another maximum builds, centered at 11 hrs and +50°. IRTM data indicate that this peak may be closer to 12 hrs in the +60° latitude range, but their coverage of local time, superb in the south, was even more limited than that of MGS in the north. After L_s 265°, northern peaks at ~9 hrs begin to occur sporadically, presumably in conjunction with strong travelling wave events.

One potentially useful subtlety to these data is the effect of the slightly noncircular orbit (370-435 km). For a circular orbit, all quadrants would have a similar and constant penetration of the limb into the fields of view, ignoring minor pitch and roll. Since the orbit is highly polar, it is still true that the sidelooking quadrants have similar penetration at a given moment. However, the fore and aft fields will sample the same latitude at times separated by about 14 minutes, and during that time, the altitude can change significantly. That means a slightly different emission angle for the B field, and thus a sampling of a range of altitudes offset from the case for the

latitude range, but their coverage of local time, superb in the south, was even more limited than that of MGS in the north. After L_s 265°, northern peaks at ~9 hrs begin to occur sporadically, presumably in conjunction with the strong travelling wave events.

There is evidence of semidiurnal variation in the north during the dusty period.

One potentially useful subtlety to these data is the effect of the slightly noncircular orbit (370-435 km). For a circular orbit, all quadrants would have a similar and constant penetration of the limb into the fields of view, ignoring minor pitch and roll. Since the orbit is highly polar, it is still true that the sidelooking quadrants have similar penetration at a given moment. However, the fore and aft fields will sample the same latitude at times separated by about 14 minutes, and during that time, the altitude can change significantly. That means a slightly different emission angle for the B field, and thus a sampling of a range of altitudes offset from the case for the opposing quadrant. This effect is most readily seen in the middle latitudes where the latitudinal gradient is highest. There is in general a positive lapse rate in the Martian atmosphere, so that deeper sampling yields higher temperatures. We have not pursued this aspect to date, because lapse rates are already well determined by the TES.

Future work will center on exploration of phenomena for which the MHSA data are well suited, particularly the diurnal variation relative to model predictions. We will compile day-night differences as maps, and make comparison in greater detail with the wealth of information coming from the TES experiment.

MHSA data are being archived for the periods used for atmospheric monitoring during aerobraking, and continuously during the mapping phase. The data are being preserved by the Atmospheres Node of the Planetary Data System.

This research was carried out at the Jet Propulsion Laboratory, California Institute of Technology, under a contract with the National Aeronautics and Space Administration. We thank the Mars Surveyor Operations Project for supporting the MHSA as a useful measurement tool. Further support was derived from the NASA Mars Data Analysis Program.

REFERENCES

Christensen, P.R., D.L. Anderson, S.C.Chase, R.T.Clancy, R.N. Clark, B.J. Conrath, H.H. Kieffer, R. O. Kuzmin, M.C. Malin, J.C. Pearl, T. L. Roush, and M.D. Smith, Results from the Mars Global Surveyor Thermal Emission Spectrometer, *Science* 279, 1692, 1998.

G. M. Keating, S.W. Bougher, R.W. Zurek, R.H. Tolson, G.J. Cancro, S.N. Noll, J.S. Parker, T.J. Schellenberg, R.W. Shane, B.L. Wilkerson, J.R. Murphy, J.L. Hollingsworth, R.M. Haberle, M. Joshi, J.C. Pearl, B.J. Conrath, M.D. Smith, R.T. Clancy, R.C. Blanchard, R.G. Wilmoth, D.F. Rault, T.Z. Martin, D.T. Lyons, P.B. Esposito, M. D. Johnston, C.W. Whetsel, C.G. Justus, and J.M. Babicke, The structure of the upper atmosphere of Mars: in situ accelerometer measurements from Mars Global Surveyor, *Science* 279, 1672, 1998.

Martin, T.Z., Mean thermal and albedo behavior of the Mars surface and atmosphere over a Martian year, *Icarus* 45, 427, 1981.

Ward, K.A., *Proc.Soc. Photo. Instrum. Eng.* 327, 67, 1982.

Wilson, R. J. and Richardson, M.I., The Martian atmosphere during the Viking mission, 1: Infrared measurements of atmospheric temperatures revisited, *Icarus* TBD, TBD, 1999.

Figure legends

Fig. 1. Fields of view of the Mars Horizon Sensor within one of the four quadrants. The differing shapes of the A and B fields permit derivation of the limb height within the B field and the radiance of the part of the planet disk covered. The output of the two A fields is ganged. The S field provides space reference data to counteract signal drift.

Fig. 2. Mars Horizon Sensor weighting functions. The amplitude of this function expresses the contribution of various levels of the atmosphere to the total signal measured by the instrument. The 0° emission angle case (nadir viewing) is relevant to much of the aerobraking data obtained; the 82° case is a mean for the part of the B field that is on the planet during the mapping phase.

Fig. 3. Comparison between MHSA on-planet signal levels and TES radiance values integrated over the MHSA filter pass band, during part of the periapsis 43 pass in 1997. The value B4 (B field DN in quadrant 4) is used for space reference during aerobraking because all the quadrant 2 fields of view are on the disk. This correlation was used to establish a calibration of the MHSA for the aerobraking period.

Fig. 4. Longitudinal variation of the latitude of steepest latitudinal temperature gradient, compiled from a series of periapsis passes during the first aerobraking period, L_s 260 to 278°. The data were measured on both the dayside of the pole, nearest to periapsis, and on the preceding nightside (downward leg) of the orbits. The latter have higher emission angle and thus refer to somewhat higher altitudes in the atmosphere. A wave 1 and 2 fit is shown for reference.

Fig. 5. Thermal effect of the Noachis dust storm. MHSA temperatures for periapsis passes 47 and 50 (November 1997, L_s 222.2 – 224.8°, a period of 97 hrs) show the broad latitudinal extent of the temperature rise associated with the raising of dust in the southern hemisphere. The two passes are offset in longitude by 20°.

Fig. 6. Selected maps of thermal behavior; seasonal range is indicated. Note similarity of equinoctial periods at bottom left and right, and south polar maximum at the southern solstice, middle right.

Fig. 7. Diurnal behavior during clear and dusty atmosphere conditions. Upper left: isothermal behavior in clear conditions; lower left: development of late afternoon peak in the south; upper right: height of dust storm season, with a late morning peak in the north; lower right: strong peak associated with travelling waves in the north.

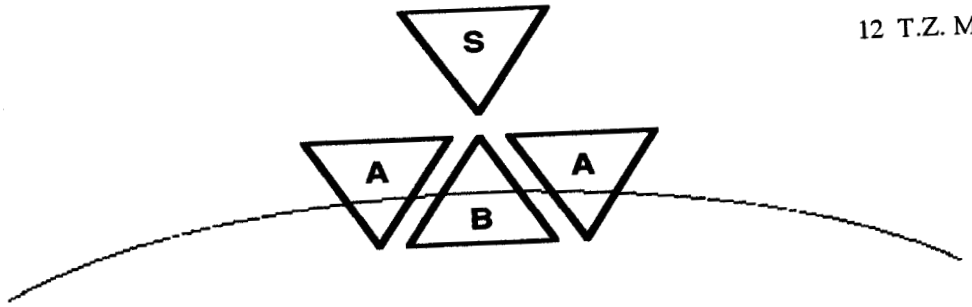
S
A
A
B

Fig. 1.

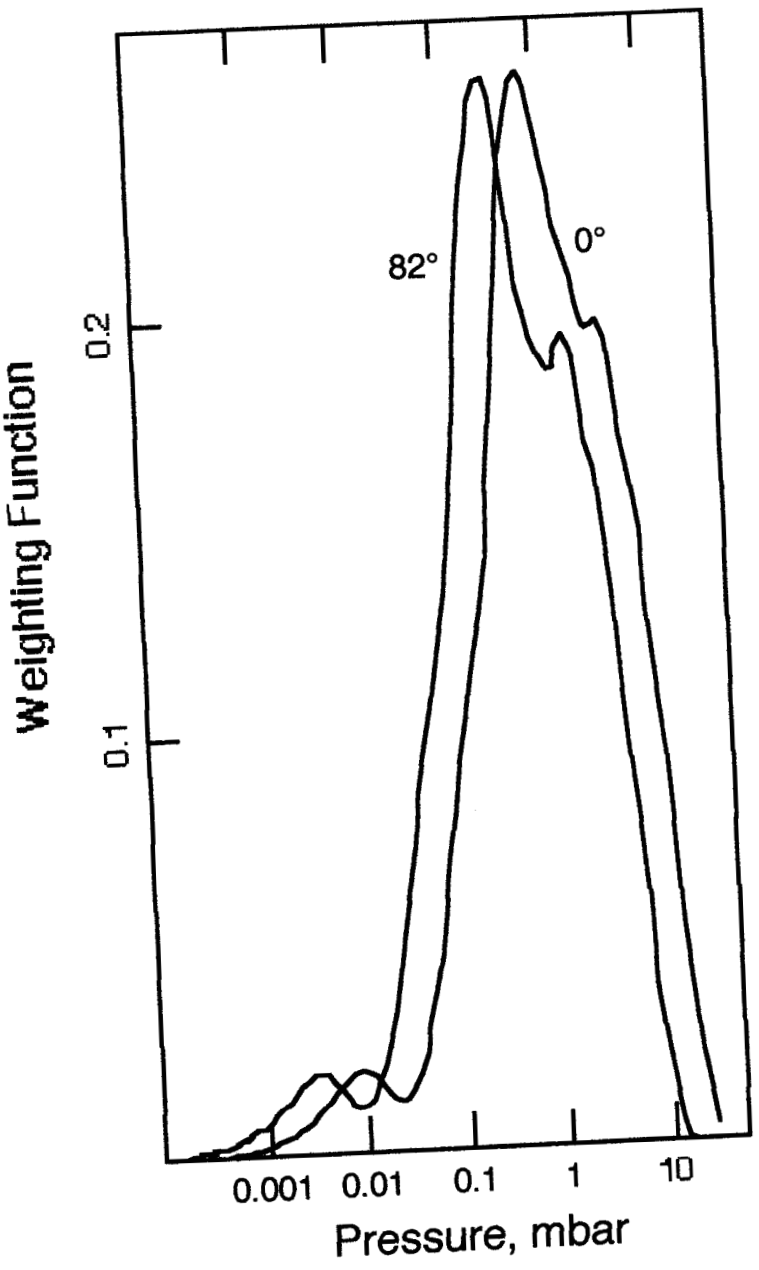
82°
0°
0.2
0.1
Weighting Function
0.001
0.01
0.1
1
10
Pressure, mbar

Fig. 2.

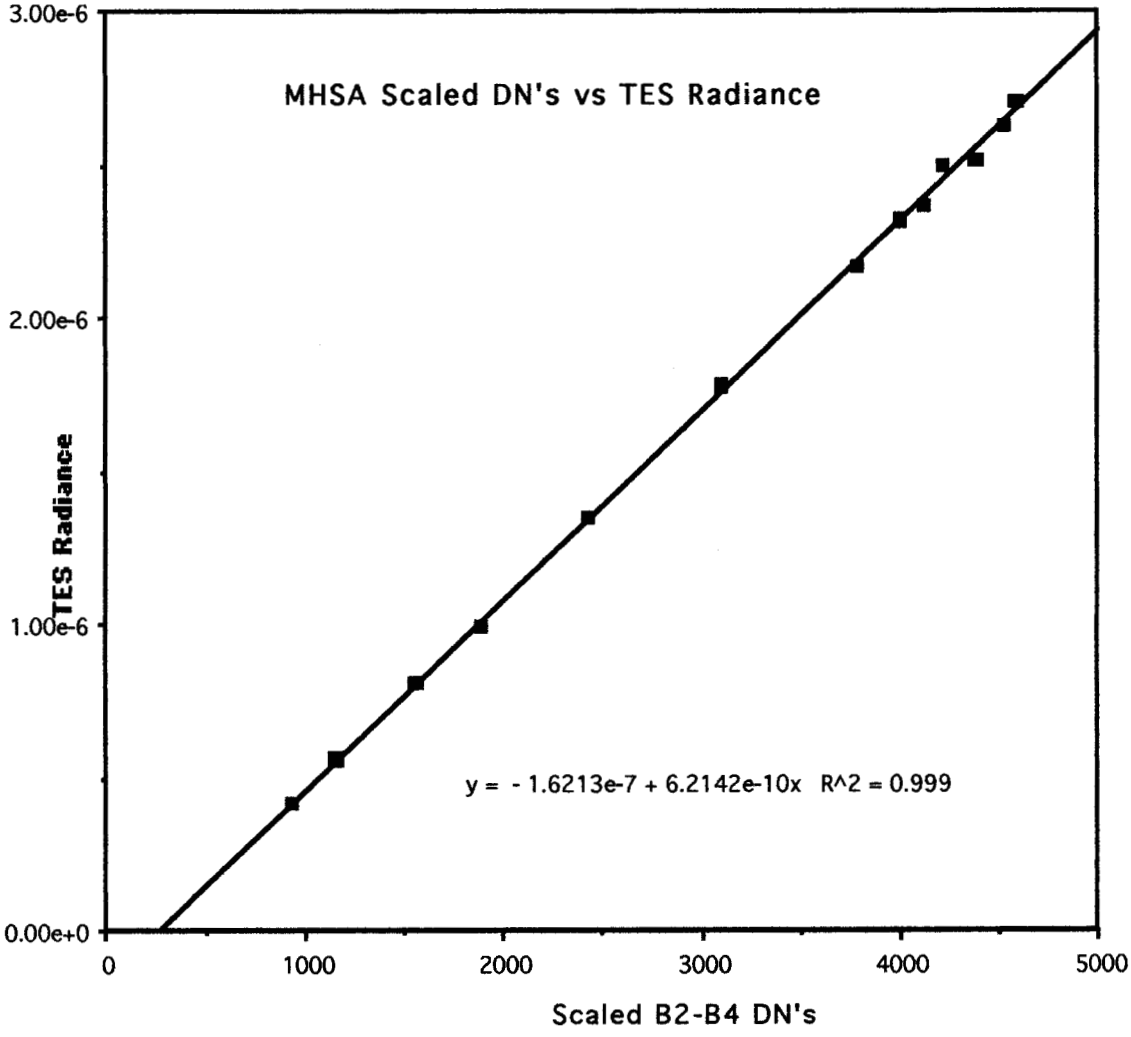
MHSA Scaled DN's vs TES Radiance
y = - 1.6213e-7 + 6.2142e-10x R^2 = 0.999
TES Radiance
Scaled B2-B4 DN's
3.00e-6
2.00e-6
1.00e-6
0.00e+0
0
1000
2000
3000
4000
5000

Fig. 3.

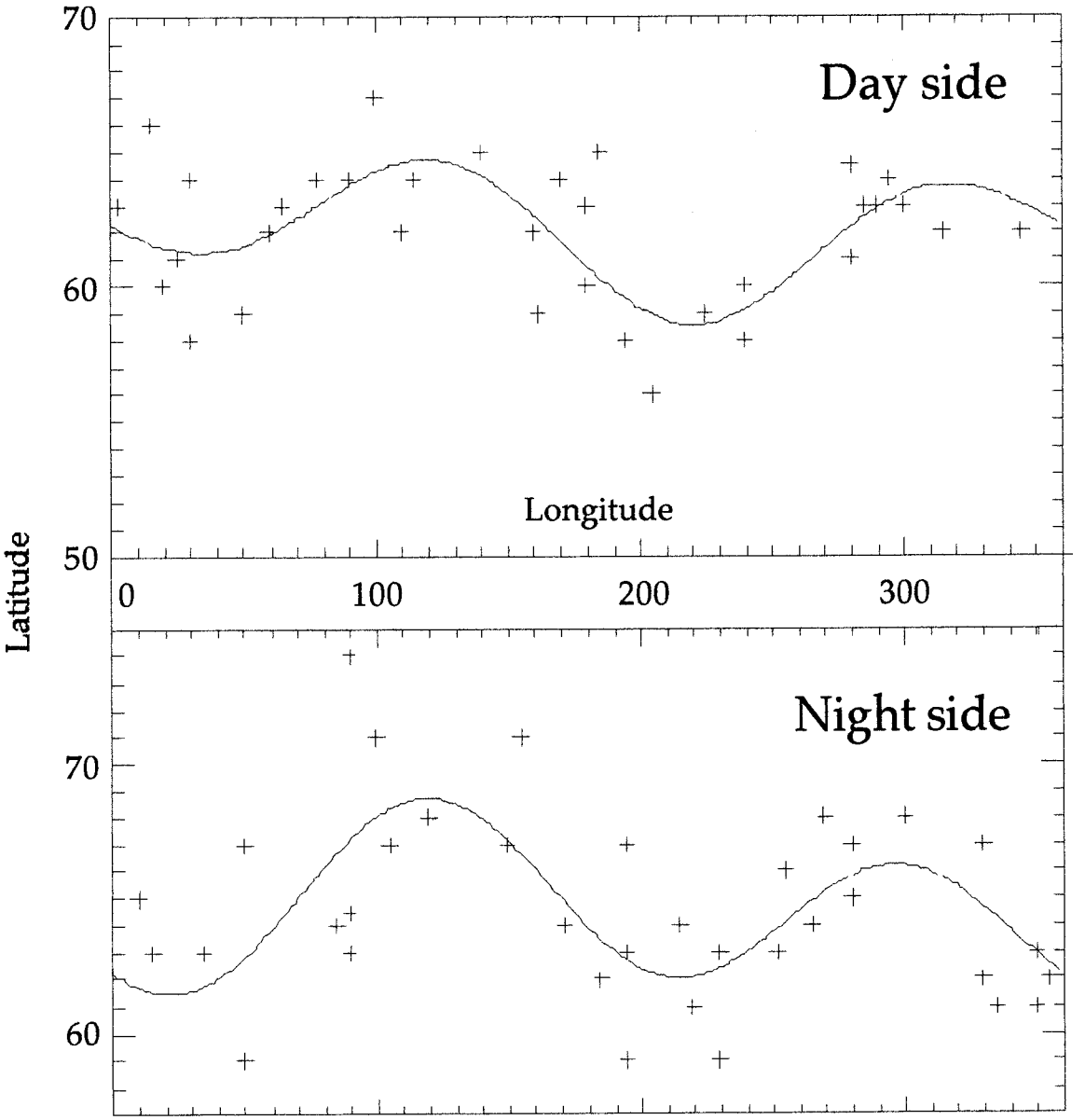
Day side
Night side
Latitude
Longitude
70
60
50
0
100
200
300
70
60

Fig. 4.

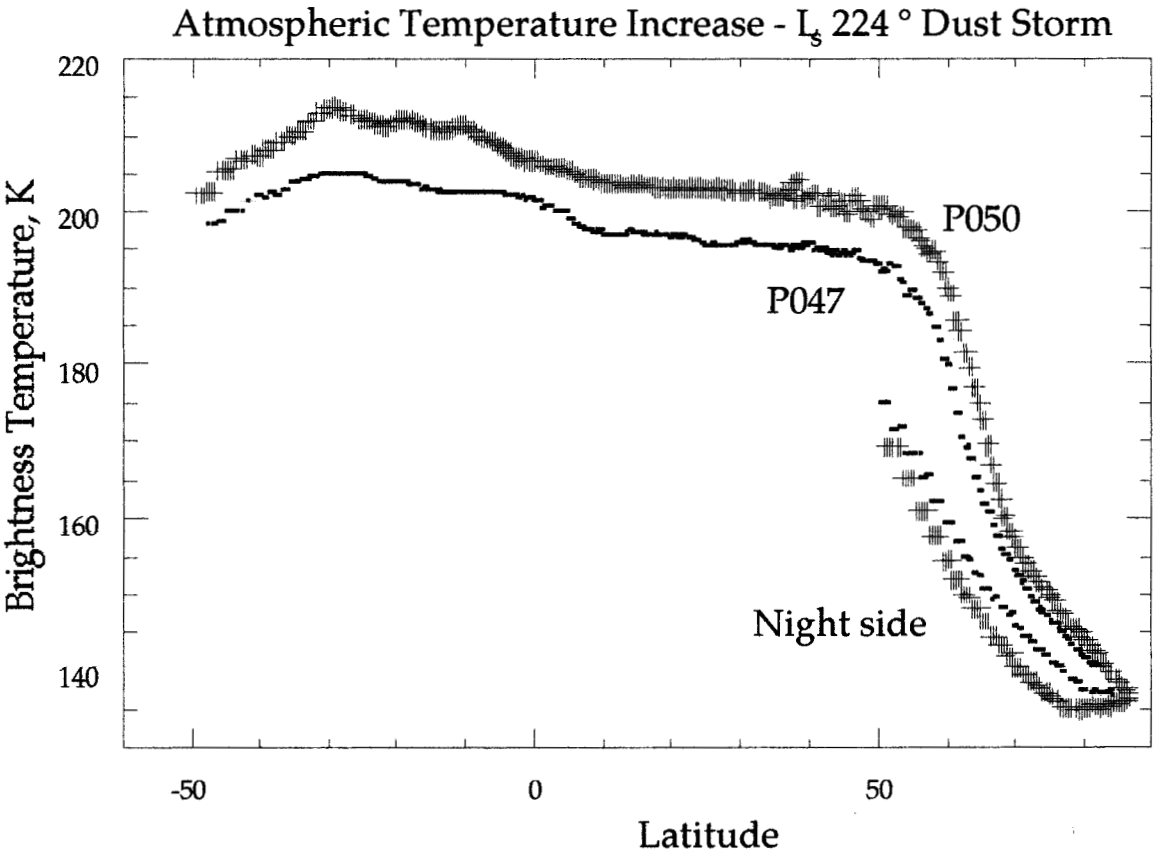
Atmospheric Temperature Increase - L_s 224 ° Dust Storm
Brightness Temperature, K
220
200
180
160
140
-50
0
50
Latitude
P050
P047
Night side

Fig. 5.

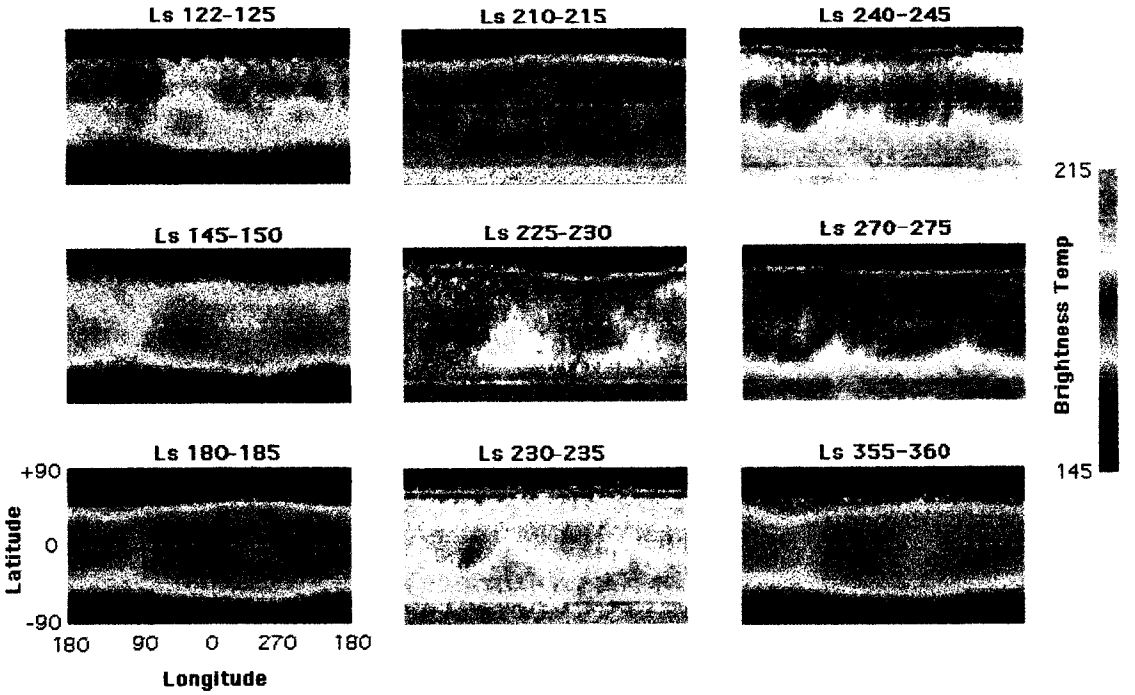
Ls 122-125
Ls 210-215
Ls 240-245
Ls 145-150
Ls 225-230
Ls 270-275
Ls 180-185
Ls 230-235
Ls 355-360
215
Brightness Temp
145
+90
0
-90
Latitude
180
90
0
270
180
Longitude

Fig. 6..

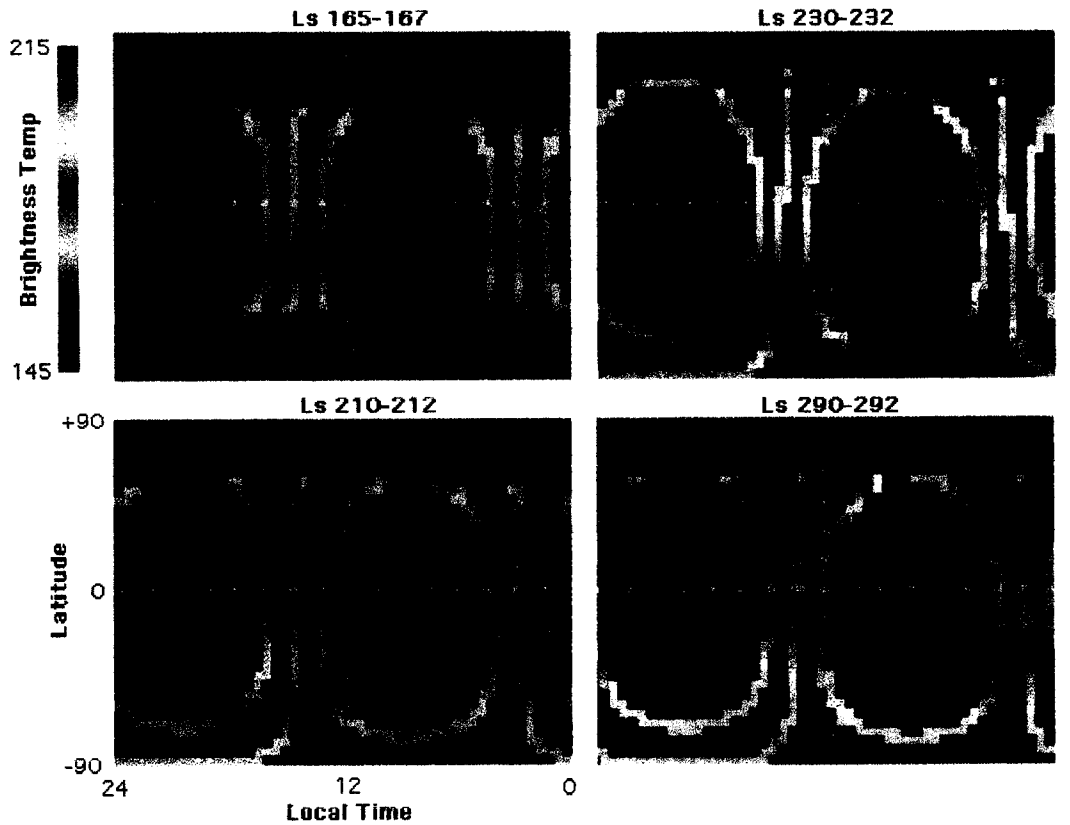
Ls 165-167
Ls 230-232
215
Brightness Temp
145
Ls 210-212
Ls 290-292
+90
0
-90
Latitude
24
12
0
Local Time

Fig. 7.